

Article

Influence of Butanol Isomerization on Photothermal Hydrogen Production over Ti@TiO₂ Core-Shell Nanoparticles

Sara El Hakim, Mathéo Bathias, Tony Chave and Sergey I. Nikitenko *

Institute for the Separation Chemistry in Marcoule (ICSM), University Montpellier, UMR 5257, CEA, CNRS, ENSCM, Marcoule, F-30207 Bagnols sur Cèze, France

* Correspondence: sergei.nikitenko@cea.fr

Abstract: In this work, we reported for the first time the effect of butanol isomerization on the photothermal production of hydrogen in the presence of a noble, metal-free Ti@TiO₂ core-shell photocatalyst. The experiments were performed in aqueous solutions of 1-BuOH, 2-BuOH, and t-BuOH under Xe lamp irradiation (vis/NIR: 8.4 W, UV: 0.6 W) at 35–69 °C. The increase in temperature significantly enhanced H₂ formation, indicating a strong photothermal effect in the studied systems. However, in dark conditions, H₂ emission was not observed even at elevated temperatures, which clearly points out the photonic origin of H₂ photothermal formation. The rate of H₂ production followed the order of 1-BuOH >> 2-BuOH > t-BuOH in the entire range of studied temperatures. In the systems with 1-BuOH and 2-BuOH, hydrogen was the only gaseous product measured online in the outlet carrier argon using mass spectrometry. By contrast, a mixture of H₂, CH₄, and C₂H₆ was detected for t-BuOH, indicating a C–C bond scission with this isomer during photocatalytic degradation. The apparent activation energies, E_a, with 1-BuOH/2-BuOH isomers (20–21 kJ·mol^{−1}) was found to be larger than for t-BuOH (13 kJ·mol^{−1}). The significant difference in thermal response for 1-BuOH/2-BuOH and t-BuOH isomers was ascribed to the difference in the photocatalytic mechanisms of these species. The photothermal effect with 1-BuOH/2-BuOH isomers can be explained by the thermally induced transfer of photogenerated, shallowly trapped electron holes to highly reactive free holes at the surface of TiO₂ and the further hole-mediated cleavage of the O–H bond. In the system with t-BuOH, another mechanism could also contribute to the overall process through hydrogen abstraction from the C–H bond by an intermediate •OH radical, leading to CH₃• group ejection. Formation of •OH radicals during light irradiation of Ti@TiO₂ nanoparticle suspension in water has been confirmed using terephthalate dosimetry. This analysis also revealed a positive temperature response of •OH radical formation.



Citation: El Hakim, S.; Bathias, M.; Chave, T.; Nikitenko, S.I. Influence of Butanol Isomerization on Photothermal Hydrogen Production over Ti@TiO₂ Core-Shell Nanoparticles. *Catalysts* **2022**, *12*, 1662. <https://doi.org/10.3390/catal12121662>

Academic Editor: Akira Nishimura

Received: 10 November 2022

Accepted: 15 December 2022

Published: 17 December 2022

Publisher's Note: MDPI stays neutral with regard to jurisdictional claims in published maps and institutional affiliations.



Copyright: © 2022 by the authors. Licensee MDPI, Basel, Switzerland. This article is an open access article distributed under the terms and conditions of the Creative Commons Attribution (CC BY) license (<https://creativecommons.org/licenses/by/4.0/>).

Keywords: photocatalysis; hydrogen production; butanol; isomers; photothermal effect; titanium

1. Introduction

Environmentally friendly industry is likely to be a dominant end-use for hydrogen as the world strives to achieve net zero by 2050 [1,2]. Catalytic processes play a key role in the production of low-carbon hydrogen [3,4]. More specifically, photocatalytic hydrogen evolution from bio-based sources, such as alcohols, has a great potential for green hydrogen production and can also be used effectively for the production of value-added aldehydes, carboxylic acids, and esters [5]. Note that, although CO₂ is also released in these processes, it is considered to be a part of a clean cycle when the sacrificial reagent has a biological origin [6]. Introducing heat into photocatalytic processes has attracted much attention in the last decade because it may significantly improve photoconversion efficiency [7,8]. However, the data about dominating photothermal mechanisms during H₂ production are still scarce in the literature. Recent studies of the H/D kinetic isotope effect revealed that the photothermal effect in the process of reforming aqueous glycerol over a Ti@TiO₂ core-shell photocatalyst is mainly attributed to the electron-hole-mediated splitting of the

O-H bond from glycerol [9]. On the other hand, the dynamics of intermediates at the catalyst surface could also contribute to the overall reaction kinetics through the entropy of activation. It was concluded that this effect reduces the influence of temperature on photocatalytic hydrogen production. Herein, we focus on photothermal H₂ production from aqueous solutions of butanol isomers in the presence of Ti@TiO₂ nanoparticles (NPs). Numerous studies of photocatalytic alcohol reforming over bare TiO₂ and noble metal-loaded TiO₂ NPs in aqueous solutions, and in a gas phase, revealed the involvement of α -H atom abstraction in the limiting stage for primary and secondary alcohol isomers, followed by the formation of aldehydes or ketones, respectively [10–13]. On the other hand, the photoreforming of t-BuOH in the gas phase over TiO₂ yields butyraldehyde as a primary product [14,15]. In aqueous solutions, photocatalytic degradation of t-BuOH over platinumized TiO₂ is accompanied by C–C bond scission and formation of an H₂, CH₄, C₂H₆ gas mixture [16]. To the best of our knowledge, the influence of butanol isomerization on photothermal H₂ production in aqueous solutions has not been reported in the literature. Meanwhile, a comparative study of butanol isomers would provide new insights onto the photothermal reaction mechanism.

2. Results and Discussion

The experiments were performed using Ti@TiO₂ core-shell NPs obtained by sonohydrothermal treatment (SHT) of metallic titanium Ti⁰ NPs in pure water. The experimental details are described in Materials and Methods. HR TEM images (Figure 1) show the quasi-spherical air-passivated Ti⁰ NPs (50–150 nm) before SHT treatment. These particles tend to exhibit a nanocrystalline shell composed of 10–20 nm anatase TiO₂ crystals after SHT treatment. Detailed analysis of Ti@TiO₂ NPs has been reported in our earlier studies [17–19]. It was shown that Ti@TiO₂ NPs provide an extended photo response in the UV/vis/NIR spectral range due to the interband/intraband transitions of the metallic core and the bandgap of the semiconducting titanium oxide shell (3.52 ± 0.01 eV [18]), thus allowing efficient solar light harvesting. Photocatalytic activity of this material was ascribed to the effective electron-hole separation between the Ti⁰ core and the nanocrystalline TiO₂ shell. This conclusion is supported by the fact that the non-coated Ti⁰ NPs do not exhibit photocatalytic activity despite strong light absorption [17,18].

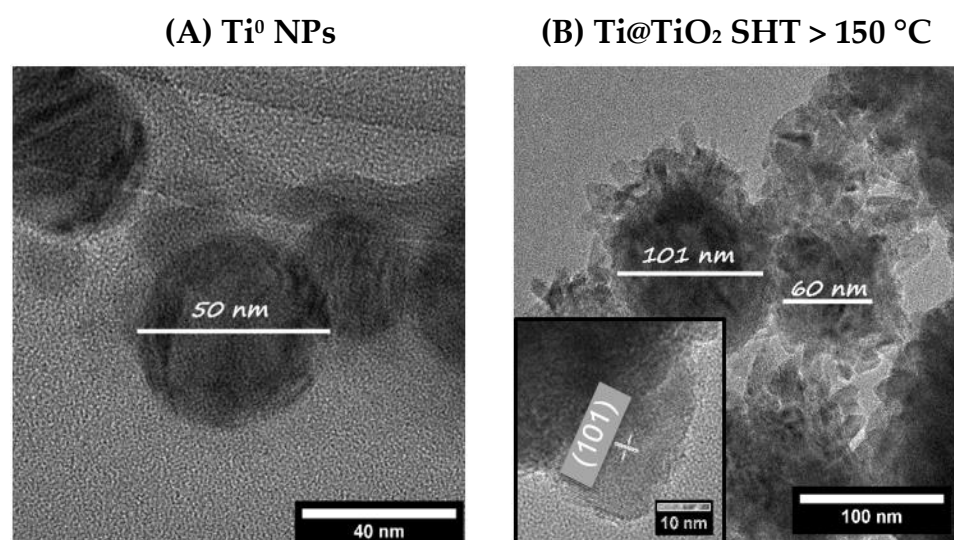


Figure 1. Typical HR TEM images of Ti⁰ (A) and Ti@TiO₂ (B) NPs. In the inset, the distance of 0.35 nm corresponds to (101) plane of TiO₂ anatase. The analysis was performed with a Jeol 2200FS (200 kV) device.

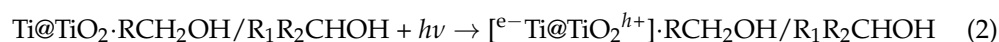
Figure 2 depicts a typical profile of H₂ emission obtained using a 0.5 M 1-BuOH aqueous solution irradiated using an Xe lamp in the presence of suspended Ti@TiO₂ NPs. The 2-BuOH and t-BuOH solutions exhibit similar behavior. A stepwise increase in the bulk temperature causes a significant stepwise increase in H₂ concentration in the outlet gas, indicating a strong photothermal effect in the studied system. However, when the light is cut off, H₂ formation is not observed even at elevated temperatures, which clearly indicates the photonic origin of H₂ formation. It should be noted that the strong evaporation of BuOH isomers does not allow us to study H₂ photothermal production at T > 69 °C.

In the entire range of the studied temperatures, the H₂ formation rate fell in the sequence of 1-BuOH >> 2-BuOH > t-BuOH as shown in Figure 3. This trend can be explained by the increased adsorption strength of primary alcohols on the metal oxide surface as compared to secondary and tertiary isomers [20]. It is worth noting that the isomers of alcohols exhibit such tendencies with many other TiO₂-based photocatalysts loaded with noble metals, M/TiO₂, where M = Pt, Pd, Au, Rh [21–23]. Table 1 summarizes the values of the apparent activation energy, E_a, calculated from Arrhenius plots obtained in the temperature range of 35–69 °C for all studied systems. Thus, it can be noticed that, despite the significant difference in reaction rate, both systems with 1-BuOH and 2-BuOH are characterized by very similar values of E_a. In addition, these values are comparable with the E_a measured previously for reforming glycerol with the same catalyst [19], which implies a similarity in the reaction mechanism for these sacrificial reagents. Earlier studies have noticed that the photothermal effect during the photolysis of glycerol with Ti@TiO₂ NPs is attributed to the thermally induced transfer of photogenerated, shallowly trapped electron holes to highly reactive free holes, h⁺, at the surface of TiO₂ [9]. Further electron-hole-mediated cleavage of the O-H bond from glycerol could lead to H₂ formation. Similarly, the photothermal H₂ production on Ti@TiO₂ in the presence of 1-BuOH/2-BuOH isomers can be expressed by the Equations (1)–(4):

Scavenger adsorption:



Photoexcitation:



Hole-mediated oxidation:



Molecular hydrogen formation:



where RCH₂OH and R₁R₂CHOH correspond to 1-BuOH and 2-BuOH, respectively. After light absorption by the catalyst, the adsorbed RCH₂OH and/or R₁R₂CHOH species are oxidized by photogenerated holes to form aldehydes and/or ketones and two protons. Molecular hydrogen is then obtained upon the reduction of produced H⁺ cations by the photogenerated electrons. It is interesting to note that the photolysis of a 1-BuOH aqueous solution in the presence of TiO₂ loaded with noble metals leads to the formation of H₂, CO₂, C₃H₈ while that of 2-BuOH leads to H₂, CO₂, C₂H₆, CH₄ in the gas phase, respectively [10,24]. In our case, H₂ was the only gaseous photocatalytic product observed for both isomers. The absence of CO₂ emissions could be related to the low adsorption of the formed aldehydes/ketones on the surface of our catalyst, thus inhibiting their further oxidation into CO₂. This conclusion is supported by the absence of solution acidification during photolysis, indicating that organic acids are not formed during the process. However, for the system with t-BuOH, the formation of CH₄ and C₂H₆ was detected at 35–52 °C, along with H₂ formation, which agrees with the observation of

CH_3^\bullet radicals during photolysis of *t*-BuOH in the gas phase over TiO_2 [14]. At higher temperatures, strong evaporation of *t*-BuOH did not allow for the proper measurements of hydrocarbons using mass spectrometry.

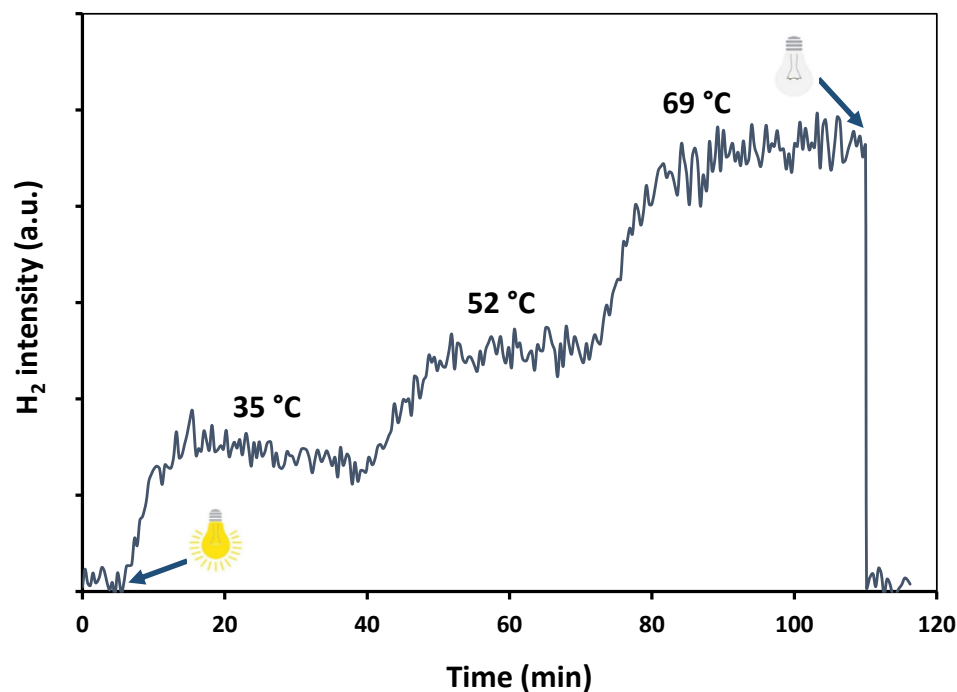


Figure 2. Typical temperature-dependent profile of H_2 emission during photolysis of 0.5 M 1-BuOH with white light of an Xe lamp under Ar flow ($45 \text{ mL}\cdot\text{min}^{-1}$) in the presence of Ti@TiO_2 NPs. H_2 was measured online in the outlet gas using mass spectrometry.

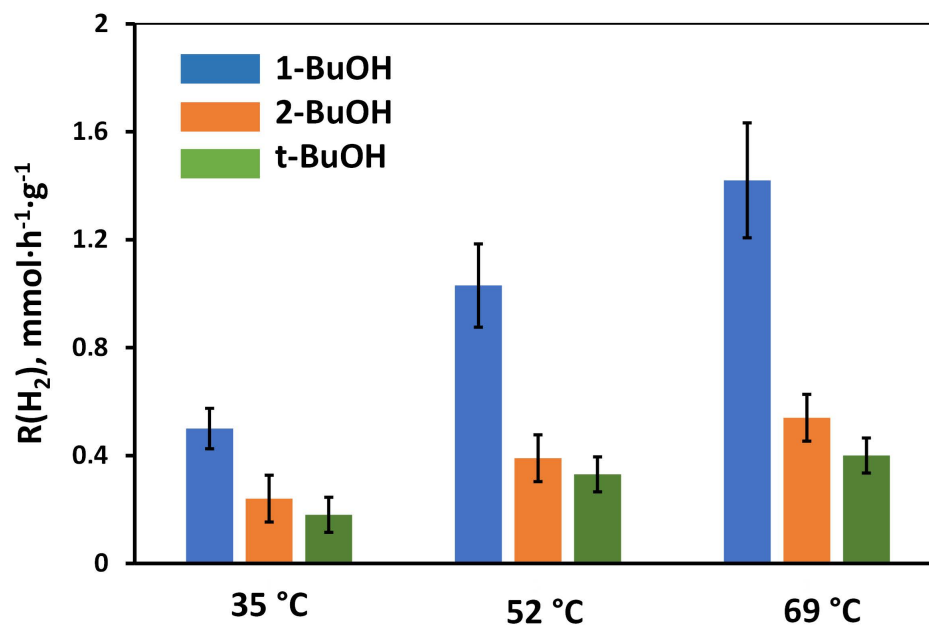


Figure 3. Rate of H_2 production as a function of bulk temperature from 0.5 M aqueous solutions of BuOH isomers irradiated with an Xe lamp (vis/NIR: 8.4 W, UV: 0.6 W) under Ar flow in the presence of Ti@TiO_2 NPs.

Table 1. The apparent activation energy of H₂ photocatalytic formation for BuOH isomers (0.5 M) irradiated with an Xe lamp in the presence of Ti@TiO₂ NPs under Ar flow.

| Alcohol | E _a , kJ·mol ⁻¹ |
|----------|---------------------------------------|
| 1-BuOH | 21 ± 2 |
| 2-BuOH | 20 ± 2 |
| t-BuOH | 13 ± 2 |
| Glycerol | 25 ± 5 * |

* Data [16].

In order to highlight the positive effect of temperature on h^+ mobility, we studied the photothermal production of $\bullet\text{OH}$ radicals in Milli-Q water in the presence of Ti@TiO₂ NPs and without the addition of any alcohols. Recently, it was reported that $\bullet\text{OH}$ radicals can be produced by oxidation of bridged O-H groups at the surface of TiO₂-based catalysts with the photogenerated h^+ [25]. Herein, the kinetics of $\bullet\text{OH}$ radical formation was studied using terephthalate dosimetry [26]. This analytical technique is based on $\bullet\text{OH}$ -induced hydroxylation of the terephthalate (TPH) ion and measurement of the formed 2-hydroxyterephthalate (2-HTPH) using fluorescence spectroscopy. The experimental details are described in Materials and Methods. Figure 4 clearly points out the acceleration of $\bullet\text{OH}$ radical formation expressed as 2-HTPH concentration with the increase in bulk temperature in accordance with the above-discussed photothermal mechanism of H₂ production. The deceleration of 2-HTPH accumulation with irradiation time is most likely related to the photocatalytic oxidation of 2-HTPH.

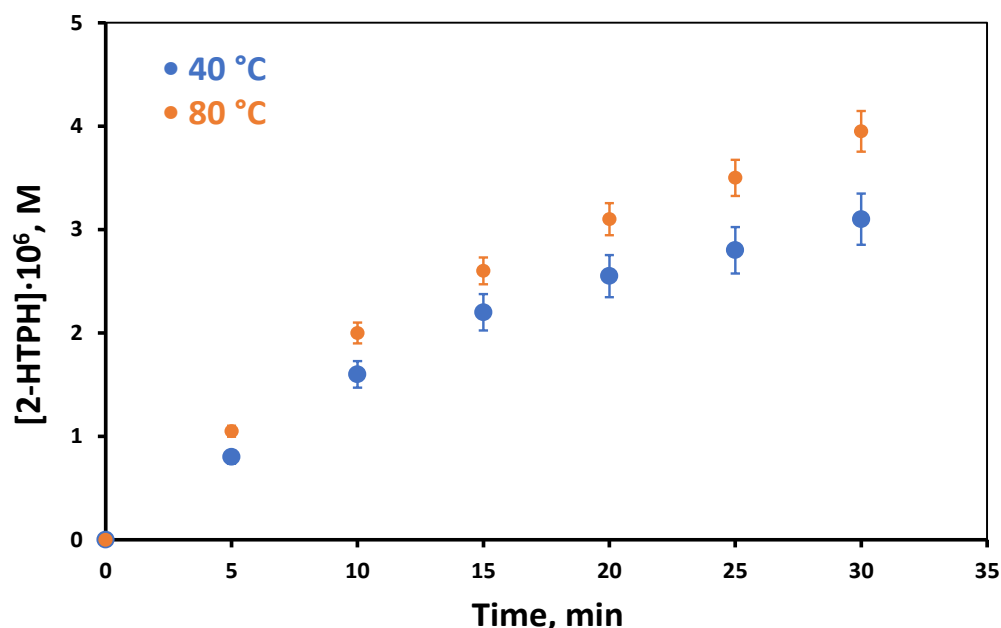
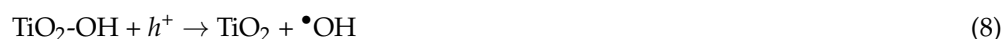
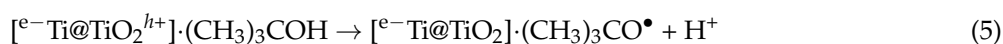


Figure 4. Kinetics of photocatalytic $\bullet\text{OH}$ radical formation as a function of bulk temperature measured using terephthalate dosimetry in the presence of Ti@TiO₂ NPs and in the absence of butanol isomers (Xe lamp, Ar flow).

On the basis of the above results, it is evident that a rather low E_a value for t-BuOH in comparison with 1-BuOH/2-BuOH isomers (Table 1) reflects the significant influence of C-C bond scission on the photothermal effect with t-BuOH. As aforementioned, the photothermal reforming of primary and secondary alcohols in the presence of TiO₂-based photocatalysts deals with the mobility of photogenerated h^+ [9,27,28]. In the system with t-BuOH, there are two possible reaction pathways for t-BuOH photoconversion: h^+ -mediated O-H bond cleavage similar to that with 1-BuOH/2-BuOH isomers (Reactions 5,6), and

hydrogen abstraction from the C-H bond by the intermediate OH^\bullet radical, leading to CH_3^\bullet group ejection (Reactions 8,9) [16]:



The secondary reactions (10,11) leading to the emission of methane and ethane could influence the production of H_2 . Actually, the E_a measured experimentally involves not only the enthalpy of activation, ΔH^\ddagger , but also the entropy of activation, ΔS^\ddagger , which is sensitive to the reorganization of the solvent network during product formation and the migration of intermediates as well. In terms of the Eyring transition state theory, the free energy of activation, ΔG^\ddagger , can be approximated as [29,30]:

$$E_a \approx \Delta G^\ddagger = \Delta H^\ddagger - T\Delta S^\ddagger \quad (12)$$

Hydrogen bonding in aqueous solutions induces the ordering of alcohol molecules at the surface of the catalyst. The ejection of the methyl group from t-BuOH would provide much stronger modification of the H-bonding network and, consequently, larger activation entropy than in the case of O-H bond cleavage for 1- and 2-BuOH isomers, which finally would lead to the drop of photothermal effect for t-BuOH.

3. Materials and Methods

3.1. Chemical Reagents

1-BuOH, 2-BuOH, t-BuOH (all > 99%, Sigma-Aldrich, St. Louis, MI, USA), terephthalic acid, TPH (99%, Acros Organics, Waltham, MA, USA), 2-hydroxyterephthalic acid, 2-HTPH (97%, Sigma-Aldrich), NaOH (98%, Alfa Aesar, Haverill, MA, USA), KH_2PO_4 (99%, Sigma-Aldrich), and Na_2HPO_4 (99%, Sigma-Aldrich) were used as received without further purification. All solutions were prepared using Milli-Q grade ultrapure water (18.2 M Ω ·cm at 25 °C). Pure Ar (99.999%) was supplied by Air Liquid.

3.2. Catalyst Preparation

Ti@TiO_2 NPs were obtained by sonohydrothermal treatment (20 kHz, 200 °C) of commercially available Ti^0 NPs (American Elements) as described previously [19]. Typically, 2 g of air-passivated Ti^0 NPs was dispersed in 50 mL of Milli-Q water using an ultrasonic bath. The suspension was then transferred into the sonohydrothermal reactor and heated at 200 °C (autogenic pressure $P = 19$ bar) under simultaneous ultrasonic treatment ($f = 20$ kHz, $P_{ac} = 17$ W) for 3 h. After cooling, the obtained particles were recovered using centrifugation, washed with deionized water, and dried at room temperature under reduced pressure.

3.3. Photocatalytic Experiments

The photocatalytic study was performed in a thermostated glass-made gas-flow cell as shown in Figure 5. The temperature inside the reactor was controlled by an external thermostat. In a typical run, 7.8 mg of photocatalyst was dispersed ultrasonically in 65 mL of an aqueous solution of alcohol before transferring it into the photoreactor. The cell used for the photocatalytic experiments was equipped with two inlets, one to purge the gas and another to measure the temperature during photothermal treatment. The argon gas

flow through the reactor was controlled by a volumetric flowmeter and kept constant at $45 \text{ mL}\cdot\text{min}^{-1}$ during the experiment. Photocatalytic experiments were carried out using the white light of an ASB-XE-175W xenon lamp. During the experiments, the lamp was placed at a distance of 8 cm away from the reactor. The light intensity delivered onto the reactor at such distance was measured with an X1-1 Optometer (Gigahertz-Optik) using UV-3710-4 (300–420 nm) and RW-3705-4 (400–1100 nm) calibrated detectors. The obtained values were normalized to the irradiated surface area, and the calculated light power was equal to 8.4 W and 0.6 W for vis/NIR and UV spectral ranges, respectively. During the photocatalytic treatment, the suspensions inside the reactor were stirred continuously, and the temperature was increased stepwise up to $69 \text{ }^\circ\text{C}$. The cell used for performing the photocatalytic experiments was also equipped with an outlet connected to a bench-top magnetic sector mass spectrometer (Thermo Scientific PRIMA BT, Waltham, MA, USA), allowing for the continuous online analysis of the produced gases. The H_2 formation was quantified using external calibration curves prepared with standard gas mixtures in argon (Air Liquide).

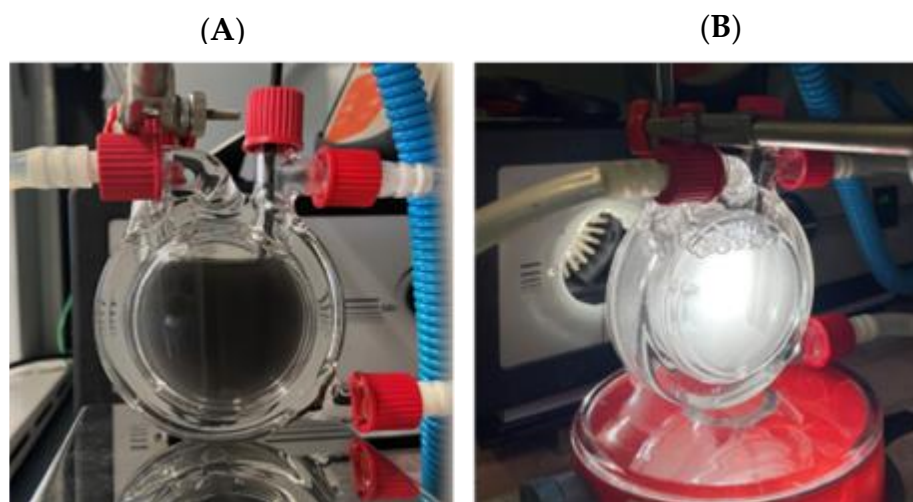


Figure 5. Image of the photocatalytic cell before (A) and during (B) illumination with xenon lamp.

3.4. Terephthalate Dosimetry

The solution for terephthalate dosimetry was prepared as follows: 332 mg of terephthalic acid was dissolved under mechanical stirring at an ambient temperature in a 500 mL buffer solution prepared with 200 mg of NaOH, 590 mg of KH_2PO_4 , and 980 mg of Na_2HPO_4 dissolved in Milli-Q water. The obtained solution was then diluted to 1 L with water. Then, 7.8 mg of photocatalyst was dispersed into 65 mL of the prepared solution using an ultrasonic bath and further introduced into the photocatalytic cell. During photolysis, sample aliquots were withdrawn from the reactor every 5 min and filtered through $0.2 \mu\text{m}$ PTFE filters. The concentration of 2-hydroxyterephthalic acid formed upon the reaction of terephthalic acid with $\bullet\text{OH}$ radicals was measured using fluorescence at 425 nm using a Fluoromax-4 device equipped with a Horiba NanoLED laser providing an excitation wavelength of 315 nm. A calibration curve has been obtained using standard solutions of 2-hydroxyterephthalic acid.

4. Conclusions

The photothermal hydrogen production from the aqueous solutions of 1-BuOH, 2-BuOH, and t-BuOH isomers studied in this work provides new insights into reaction mechanisms. The experiments were performed using innovative, noble, metal-free core-shell Ti@TiO_2 nanoparticles obtained through hydrothermal oxidation of metallic titanium nanoparticles assisted by power ultrasound. We found that the isomerization of butanol strongly influences the kinetics of photocatalytic hydrogen evolution and its thermal response. The 1-BuOH isomer exhibits the highest H_2 formation rate, which corroborates

with the strongest adsorption of 1-BuOH at the surface of TiO₂ compared to other butanol isomers. Analysis of the gaseous products revealed a significant difference between 1-BuOH/2-BuOH and t-BuOH. Photolysis of 1-BuOH/2-BuOH solutions yields solely H₂ as a gaseous photocatalytic product without emission of CO₂ or hydrocarbons. However, the photocatalytic degradation of t-BuOH leads to the formation of H₂, CH₄, and C₂H₆ indicating the scission of the C–C bond for tertiary isomers. A similar trend is observed in the thermal response of the photocatalytic H₂ formation. The apparent activation energies, E_a, are very similar for 1-BuOH and 2-BuOH isomers (20–21 kJ·mol^{−1}), and are also fairly close to that of glycerol measured in our earlier studies with the same catalyst. On the other hand, the E_a value for t-BuOH is much lower (13 kJ·mol^{−1}), indicating a weak photothermal effect for this isomer. This difference has been attributed to the more complex mechanism in the case of tertiary isomers involving a large number of intermediates and the contribution of photogenerated •OH radicals to the degradation of t-BuOH. Formation of •OH radicals during photoexcitation of Ti@TiO₂ nanoparticles was confirmed using terephthalate dosimetry.

Author Contributions: Conceptualization, S.I.N.; methodology, S.E.H. and T.C.; formal analysis, S.I.N., S.E.H. and T.C.; investigation, S.E.H. and M.B.; data curation, S.E.H. and T.C.; writing—original draft preparation, S.E.H. and M.B.; writing—review and editing, S.I.N. and S.E.H.; visualization, S.E.H. and S.I.N.; supervision, S.I.N. All authors have read and agreed to the published version of the manuscript.

Funding: This research received no external funding.

Data Availability Statement: The data presented in this study are available in the article.

Conflicts of Interest: The authors declare no conflict of interest.

References

1. Abeab, J.O.; Popoola, A.P.I.; Ajenifuja, E.; Popoola, O.M. Hydrogen energy, economy and storage: Review and recommendation. *Int. J. Hydrogen Energy* **2019**, *44*, 15072–15086. [\[CrossRef\]](#)
2. Oureshi, F.; Yusuf, M.; Kamyab, H.; Zaidi, S.; Khalil, M.J.; Khan, M.A.; Alam, M.A.; Masood, F.; Bazli, L.; Chelliapan, S.; et al. Current trends in hydrogen production, storage and applications in India: A review. *Sustain. Energy Technol. Assess.* **2022**, *53*, 102677.
3. Voiry, D.; Shin, H.S.; Loh, K.P.; Chhowalla, M. Low-dimensional catalysts for hydrogen evolution and CO₂ reduction. *Nat. Rev. Chem.* **2018**, *2*, 0105. [\[CrossRef\]](#)
4. Qureshi, F.; Yusuf, M.; Kamyab, H.; Vo, D.-V.N.; Chelliapan, S.; Joo, S.-W.; Vasseghian, Y. Latest eco-friendly avenues on hydrogen production towards a circular bioeconomy: Current challenges, innovative insights, and future perspectives. *Renew. Sustain. Energy Rev.* **2022**, *168*, 112916. [\[CrossRef\]](#)
5. Navarro, R.M.; Sanchez-Sanchez, M.C.; Alvarez-Galvan, M.C.; Valle, F.D.; Fierro, J.L.G. Hydrogen production from renewable sources: Biomass and photocatalytic opportunities. *Energy Environ. Sci.* **2009**, *2*, 35–54. [\[CrossRef\]](#)
6. Qureshi, F.; Yusuf, M.; Pasha, A.A.; Khan, H.W.; Imteyaz, B.; Irshad, K. Sustainable and energy efficient hydrogen production via glycerol reforming technique: A review. *Int. J. Hydrogen Energy* **2022**, *47*, 41397–41420. [\[CrossRef\]](#)
7. Kollmannsberger, S.L.; Walenta, C.A.; Courtois, C.; Tschurl, M.; Heiz, U. Thermal control of selectivity in photocatalytic, water-free alcohol photoreforming. *ACS Catal.* **2018**, *8*, 11076–11084. [\[CrossRef\]](#)
8. Fang, S.; Hu, Y.H. Thermo-photo catalysis: A whole greater than the sum of its parts. *Chem. Soc. Rev.* **2022**, *51*, 3609–3647. [\[CrossRef\]](#)
9. El Hakim, S.; Chave, T.; Nikitenko, S.I. Deciphering the reaction mechanisms of photothermal hydrogen production using H/D kinetic isotope effect. *Cat. Sci. Technol.* **2022**, *12*, 5252–5256. [\[CrossRef\]](#)
10. Linsebigler, A.L.; Lu, G.Q.; Yates, J.T. Photocatalysis on TiO₂ surfaces—Principles, mechanisms, and selected results. *Chem. Rev.* **1995**, *95*, 735–758. [\[CrossRef\]](#)
11. Panayotov, D.A.; Morris, J.R. Surface chemistry of Au/TiO₂: Thermally and photolytically activated reactions. *Surf. Sci. Rep.* **2016**, *71*, 77–271. [\[CrossRef\]](#)
12. Osterloh, F.E. Photocatalysis versus photosynthesis: A sensitivity analysis of devices for solar energy conversion and chemical transformations. *ACS Energy Lett.* **2017**, *2*, 445–453. [\[CrossRef\]](#)
13. Fabian, D.M.; Hu, S.; Singh, N.; Houle, F.A.; Hisatomi, T.; Domen, K.; Osterloh, F.E.; Ardo, S. Particle suspension reactors and materials for solar-driven water splitting. *Energy Environ. Sci.* **2015**, *8*, 2825–2850. [\[CrossRef\]](#)
14. Walenta, C.A.; Kollmannsberger, S.L.; Courtois, C.; Tschurl, M.; Heiz, U. Photocatalytic selectivity switch to C–C scission: α -methyl ejection of tert-butanol on TiO₂(110). *Phys. Chem. Chem. Phys.* **2018**, *20*, 7105–7111. [\[CrossRef\]](#)

15. Courtois, C.; Walenta, C.A.; Tschurl, M.; Heiz, U.; Friend, C.M. Regulating photochemical selectivity with temperature: Isobutanol on TiO₂(110). *J. Am. Chem. Soc.* **2020**, *142*, 13072–13080. [[CrossRef](#)]
16. Nishimoto, S.; Ohtani, B.; Shirai, H.; Kagiya, T. Photocatalytic degradation and dimerization of t-butyl alcohol by aqueous suspension of platinized titanium dioxide. *J. Chem. Soc. Perkin Trans.* **1986**, *2*, 661–665. [[CrossRef](#)]
17. Nikitenko, S.I.; Chave, T.; Cau, C.; Brau, H.-P.; Flaud, V. Photothermal hydrogen production using noble-metal-free Ti@TiO₂ core-shell nanoparticles under visible-NIR light irradiation. *ACS Catal.* **2015**, *5*, 4790–4795. [[CrossRef](#)]
18. Nikitenko, S.I.; Chave, T.; Le Goff, X. Insights into the photothermal hydrogen production from glycerol aqueous solutions over noble metal-free Ti@TiO₂ core-shell nanoparticles. *Part. Part. Syst. Charact.* **2018**, *35*, 1800265. [[CrossRef](#)]
19. El Hakim, S.; Chave, T.; Nada, A.A.; Roualdes, S.; Nikitenko, S.I. Tailoring noble metal-free Ti@TiO₂ photocatalyst for boosting photothermal hydrogen production. *Front. Catal.* **2021**, *1*, 669260. [[CrossRef](#)]
20. López-Tendallo, F.J.; Hidalgo-Carrillo, J.; Montes-Jiménez, V.; Sánchez-López, E.; Urbano, F.J.; Marinas, A. Photocatalytic production of hydrogen from binary mixtures of C-3 alcohols on Pt/TiO₂: Influence of alcohol structure. *Catal. Today* **2019**, *328*, 2–7. [[CrossRef](#)]
21. López, C.R.; Pulido Melián, E.; Ortega Méndez, J.A.; Santiago, D.E.; Doña Rodríguez, J.M.; González Díaz, O. Comparative study of alcohols as sacrificial agents in H₂ production by heterogenous photocatalysis using Pt/TiO₂ catalysts. *J. Photochem. Photobiol. A Chem.* **2015**, *312*, 45–54. [[CrossRef](#)]
22. Yasuda, M.; Matsumoto, T.; Yamashita, T. Sacrificial hydrogen production over TiO₂-based photocatalysis: Polyols, carboxylic acids, and saccharides. *Renew. Sustain. Energy Rev.* **2018**, *81*, 1627–1635. [[CrossRef](#)]
23. Kennedy, J.; Bahruji, H.; Bowker, M.; Davies, P.R.; Bouleglimat, E.; Issarapanacheewin, S. Hydrogen generation by photocatalytic reforming of potential biofuels: Polyols, cyclic alcohols, and saccharides. *J. Photochem. Photobiol. A Chem.* **2018**, *356*, 451–456. [[CrossRef](#)]
24. Bahruji, H.; Bowker, M.; Davies, P.R.; Pedrono, F. New insights into the mechanism of photocatalytic reforming on Pd/TiO₂. *Appl. Catal. B Environ.* **2011**, *107*, 205–209. [[CrossRef](#)]
25. Nosaka, Y.; Nosaka, A. Understanding hydroxyl radical (\bullet OH) generation process in photocatalysis. *ACS Energy Lett.* **2016**, *1*, 356–359. [[CrossRef](#)]
26. Mark, G.; Tauber, A.; Laupert, R.; Schuchmann, H.-P.; Schulz, D.; Mues, A.; von Sonntag, C. OH-radical formation by ultrasound in aqueous solution. Part II: Terephthalate and Fricke dosimetry and the influence of various conditions on the sonolytic yield. *Ultrason. Sonochem.* **1998**, *5*, 41–52. [[CrossRef](#)]
27. Bahnemann, D.W.; Hilgendorff, M.; Memming, R. Charge carrier dynamics at TiO₂ particles: Reactivity of free and trapped holes. *J. Phys. Chem. B* **1997**, *101*, 4265–4275. [[CrossRef](#)]
28. Kim, G.; Choi, H.J.; Kim, H.; Kim, J.; Monllor-Satoca, D.; Kim, M.; Park, H. Temperature-boosted photocatalytic H₂ production and charge transfer kinetics on TiO₂ under UV and visible light. *Photochem. Photobiol. Sci.* **2016**, *15*, 1247–1253. [[CrossRef](#)]
29. Eyring, H. The activated complex in chemical reactions. *J. Chem. Phys.* **1935**, *3*, 107–115. [[CrossRef](#)]
30. Jain, P.; Yu, S. Isotope effects in plasmonic photosynthesis. *Angew. Chem. Int. Ed.* **2020**, *59*, 22480–22483.